Impact of Linear Prediction Coefficients on Totally Blind APP Channel Estimation

Marc C. Necker[1], Frieder Sanzi[2]

[1] Institute of Communication Networks and Computer Engineering, University of Stuttgart, Pfaffenwaldring 47, D-70569 Stuttgart, Germany, necker@ikr.uni-stuttgart.de, Tel.: +49 711 685 7963, Fax: +49711 685 7983

[2] Institute of Telecommunications, University of Stuttgart, Pfaffenwaldring 47, D-70569 Stuttgart, Germany, sanzi@inue.uni-stuttgart.de, Tel.: +49 711 685 7941, Fax: +49 711 685 7929

Abstract

Totally blind APP channel estimation is based on the A Posteriori Probability (APP) calculation algorithm. Asymmetrical modulation schemes are used in order to resolve the phase ambiguity with no need for any pilot or reference symbols. In OFDM-systems, the two-dimensional channel estimation is performed by applying a concatenation of two one-dimensional APP estimators for frequency and time direction in combination with an iterative estimation and decoding loop. Linear filters are used to predict the channel transfer function while traversing the trellis of the APP estimator. In this paper, we study the influence which the coefficients of these predictors have on the channel estimation result. We compare the performance of ideal predictors with the performance of predictors with coefficients based on optimal channel statistics and averaging. We study the behavior of the the iterative estimation and decoding loop using the Extrinsic Information Transfer (EXIT) Chart and evaluate the performance of the algorithm with respect to the BER.

1 Introduction

In OFDM-systems, channel estimation for coherent demodulation of data symbols can conveniently be done using a two-dimensional grid of pilot symbols [1]. This concept was successfully applied in Digital Video Broadcasting – Terrestrial (DVB–T) [2], for example. The drawback of pilot-based channel estimation is the overhead introduced by the pilot symbols, which reduces the spectral efficiency of the system. In the case of DVB-T, the overhead is more than 10%.

The amount of pilot symbols can dramatically be reduced using the channel estimation method presented in [3]. The authors base their algorithm on the calculation of the A Posteriori Probability APP and estimate the channel transfer function (CTF) by concatenating two one-dimensional APP estimators in frequency and time direction, respectively. Furthermore, the APP channel estimator can be embedded in an iterative decoding loop with a soft in/soft out decoder.

Blind channel estimation algorithms have gained attention, as they are capable of estimating the channel transfer function without the need for pilot symbols. Most research on this subject has focused on methods based on second or higher order statistics. However, time varying propagation conditions in mobile communication systems make these approaches unsuitable, since they converge slowly. Additionally, a phase ambiguity is introduced, which makes at least one reference symbol necessary to resolve.

In [4] the authors present a fast converging blind channel estimator based on the Maximum Likelihood principle. The algorithm recovers the amplitude and phase of a channel without the need for any reference symbols by combining modulation schemes, such as QPSK and 3-PSK, even in mobile environments.

The concept of totally blind channel estimation and APP channel estimation was combined in [5]. Blind channel estimation was achieved with rapidly varying mobile channels. Pilot symbols were completely avoided, and the phase ambiguity of the channel estimate was resolved by using an asymmetrical 8-QAM modulation scheme.

In [5], the predictors which are needed for traversing the trellis in the APP estimators had optimal linear prediction coefficients, which is very difficult to achieve. In this paper, we investigate the influence of the prediction coefficients. We compare different sets of prediction coefficients based on averaging and optimal channel statistics with the prediction coefficients used in [5]. In addition to the asymmetrical 8-QAM modulation scheme considered in [5], the advantages and trade-offs of using an asymmetrical 8-PSK modulation scheme are discussed.

This paper is structured as follows. Section 2 presents the system model and gives an introduction to totally blind APP channel estimation. In section 3, three different possibilities to determine the coefficients of the linear predictors are given. Finally, section 4 discusses the simulation results.

in Proc. 5th International ITG Conference on Source and Channel Coding (SCC), Erlangen, Germany, January 2004, pp. 317-324.

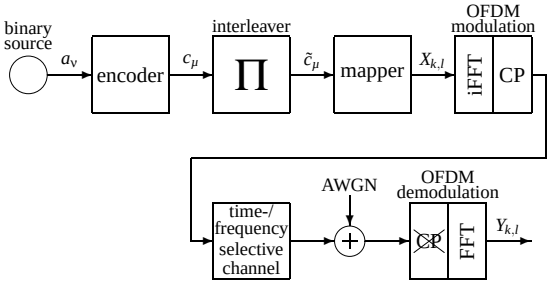

Fig. 1: Transmitter and channel model.

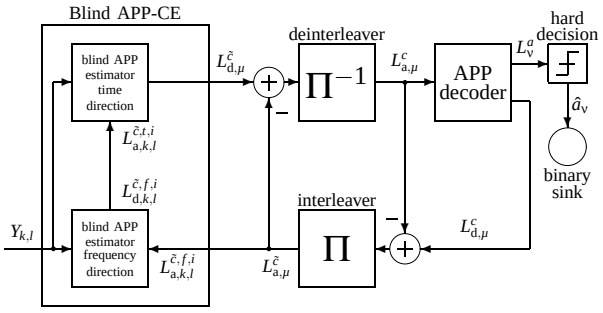

Fig. 2: Receiver with iterative blind APP channel estimation.

2 System Model

2.1 Transmitter and Receiver

We investigate an OFDM-system with $K = 1000$ subcarriers having a carrier-spacing of $\Delta f = 4\,\mathrm{kHz}$ and an OFDM-symbol duration (useful part plus guard interval) of $T_\mathrm{s} = 312.5\,\mu\mathrm{s}$. For the blockwise transmission we combine $L = 100$ successive OFDM symbols. The signal from the binary source is convolutionally encoded and interleaved as shown in Fig. 1. After interleaving, three successive coded bits are grouped and mapped onto an 8-ary symbol $X_{k,l}$. The signal $X_{k,l}$ is modulated onto K orthogonal subcarriers by an iFFT-block. Finally, a cyclic prefix of length 1/4 is inserted.

We obtain the received 8-ary signal constellation points $Y_{k,l}$ after removal of the cyclic prefix and OFDM demodulation:

$$Y_{k,l} = H_{k,l} \cdot X_{k,l} + N_{k,l}, \tag{1}$$

where l is the OFDM symbol index, k is the subcarrier index and $N_{k,l}$ are statistically i.i.d. complex Gaussian noise variables with component-wise noise power $\sigma_N^2 = N_0/2$. The $H_{k,l}$ are sample values of the CTF:

$$H_{k,l} = H(k \cdot \Delta f, l \cdot T_\mathrm{s}) \tag{2}$$

At the receiver, a blind iterative APP-CE is applied [5]. The signal $Y_{k,l}$ is fed to the blind APP-CE stage as shown in Fig. 2. This stage outputs log-likelihood ratios (L-values) on the transmitted coded bits which are deinterleaved and decoded in an APP decoder. Iterative channel estimation and decoding is performed by feeding back extrinsic information on the coded bits; after interleaving it becomes the *a-priori* knowledge to the blind APP-CE stage. The APP-CE stage is explained in detail in section 2.3.

In the encoder and decoder, we use a recursive systematic convolutional code with feedback polynomial $G_\mathrm{r} = 037_8$, feed-forward polynomial $G = 023_8$, memory 4 and code rate $R_\mathrm{c} = 0.5$. Note that in the following all E_b/N_0-values are given with respect to the overall information rate

$$R = R_\mathrm{c} \cdot R_\mathrm{g} = 0.4\,, \tag{3}$$

whereby R_g considers the redundancy introduced by the cyclic prefix:

$$R_\mathrm{g} = \frac{1}{\Delta f \cdot T_\mathrm{s}} = 0.8 \tag{4}$$

2.2 Channel Model

For the performance evaluation of the blind channel estimator we assumed a frequency-selective fading channel according to a wide-sense stationary uncorrelated scattering (WSSUS) model. The WSSUS channel was simulated according to the model introduced in [6], which describes the channel's time-variant impulse response as

$$h(\tau,t) = \lim_{Z\to\infty} \frac{1}{\sqrt{Z}} \sum_{m=1}^{Z} e^{j\theta_m} e^{j2\pi f_{\mathrm{D}m} t} \delta(\tau - \tau_m)\,. \tag{5}$$

The Fourier-Transform of equation (5) with respect to τ yields the channel's time-variant frequency response:

$$H(f,t) = \lim_{Z\to\infty} \frac{1}{\sqrt{Z}} \sum_{m=1}^{Z} e^{j\theta_m} e^{j2\pi f_{\mathrm{D}m} t} e^{-j2\pi f \tau_m}\,. \tag{6}$$

For each of the Z paths, the phase-shift θ_m, the Doppler-shift $f_{\mathrm{D}m}$ and the delay τ_m are randomly chosen from the corresponding probability density function (pdf) $p_\theta(\theta)$, $p_{f_\mathrm{D}}(f_\mathrm{D})$ or $p_\tau(\tau)$ of the channel model [6]. For the simulations, the number of paths was chosen to be $Z = 100$, which is a good tradeoff between simulation speed and accuracy.

We use a channel model where the phase θ is uniformly distributed between 0 and 2π. For the delay τ we assume an exponential pdf

$$p_\tau(\tau) = \begin{cases} \frac{\mathrm{e}^{-\tau/\tau_\mathrm{rms}}}{\tau_\mathrm{rms}\left(1-\mathrm{e}^{-\tau_\mathrm{max}/\tau_\mathrm{rms}}\right)} & 0 \le \tau \le \tau_\mathrm{max} \\ 0 & \text{otherwise} \end{cases}, \tag{7}$$

whereby τ_max is the channel delay spread. τ_rms is chosen such that $p_\tau(\tau_\mathrm{max})/p_\tau(0) = 1/1000$. The pdf of the Doppler frequency is assumed to be of Jakes' type

$$p_{f_\mathrm{D}}(f_\mathrm{D}) = \begin{cases} \frac{1}{\pi f_{\mathrm{D}\max}\sqrt{1-\left(f_\mathrm{D}/f_{\mathrm{D}\max}\right)^2}} & |f_\mathrm{D}| < f_{\mathrm{D}\max} \\ 0 & \text{otherwise} \end{cases}, \tag{8}$$

whereby $f_{\mathrm{D}\max}$ is the maximal Doppler shift.

With these assumptions the complex auto-correlation

function of $H(f,t)$ in frequency direction is given by

$$R_{f;\Delta k} = \frac{1 - e^{-\tau_{\max}(\frac{1}{\tau_{\rm rms}} + j2\pi\cdot\Delta k\cdot\Delta f)}}{(1 - e^{-\frac{\tau_{\max}}{\tau_{\rm rms}}})\cdot(1 + j2\pi\cdot\Delta k\cdot\Delta f\cdot\tau_{\rm rms})}\ , \quad (9)$$

whereby Δk is the difference of two discrete frequency indexes. For the auto-correlation function of $H(f,t)$ with respect to t we obtain

$$R_{t;\Delta l} = J_0(2\pi f_{\rm D_{max}}\cdot\Delta l\cdot T_{\rm s})\ . \quad (10)$$

Δl is the difference of two discrete time indexes and J_0 is the Bessel function of zero order. We can compute the expected value

$$\mathrm{E}\left\{H_{k,l}\cdot H^*_{k',l'}\right\} = R_{f;(k-k')}\cdot R_{t;(l-l')}\ , \quad (11)$$

whereby * denotes the conjugate complex operation. Please refer to [6] and [7] for the derivation of (9) – (11).

2.3 Iterative totally blind APP Channel Estimation

The two-dimensional blind APP channel estimator consists of one estimator for frequency and time direction, respectively [3]. The estimation algorithm exploits the time and frequency continuity of the CTF at the receiver. Blind APP-CE is possible using asymmetrical modulation schemes [5].

For one-dimensional APP estimation, the symbol-by-symbol MAP-algorithm is applied to an appropriately chosen metric. To help understanding, the symbols $X_{k,l}$ at the transmitter in Fig. 1 can be thought of being put into a virtual shift register at the output of the mapper, as sketched in Fig. 3. Due to this "artificial grouping", the corresponding trellis exploits the time and frequency continuity of the CTF at the receiver.

At frequency index k, the APP estimation in frequency direction is characterized for OFDM symbol l_0 with $0 \le l_0 \le L-1$ by the metric increment

$$\gamma_k = -\frac{|Y_{k,l_0} - \hat{H}^f_{k,l_0}\cdot\hat{X}_{k,l_0}|^2}{2\cdot\sigma_f^2} + \sum_{i=0}^{2} d^i_{k,l_0}\cdot L^{\tilde{c},f,i}_{\mathrm{a},k,l_0} \quad (12)$$

with estimated channel coefficient

$$\hat{H}^f_{k,l_0} = \sum_{i=1}^{m_f} u_{f,i}\cdot\frac{Y_{k-i,l_0}}{\hat{X}_{k-i,l_0}}\ . \quad (13)$$

The $\hat{X}_{k,l_0}$ denote the hypothesized transmitted data symbol according to the trellis structure. The $L^{\tilde{c},f,i}_{\mathrm{a},k,l_0}$ in (12) are the *a-priori* L-values of the coded bits

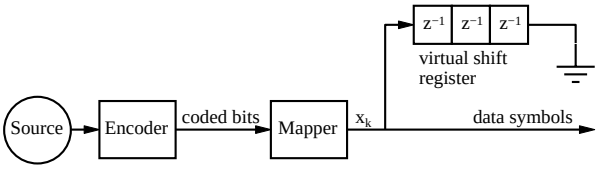

Fig. 3: Feeding symbols into the virtual shift register

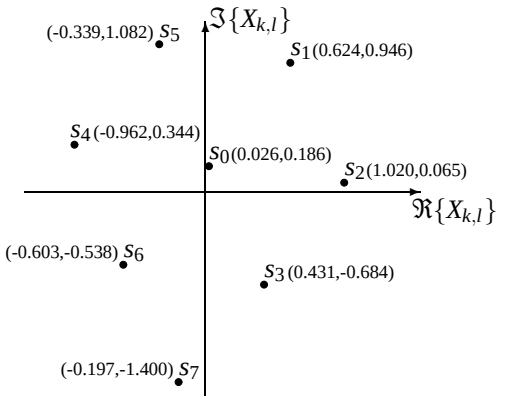

Fig. 4: Minimum-error 8-ary modulation scheme.

$\tilde{c}_\mu$ which are fed to the APP estimator in frequency direction. The bits d^0_{k,l_0}, d^1_{k,l_0} and d^2_{k,l_0} in the sum in (12) result from the hard demapping of $\hat{X}_{k,l_0}$. The calculation of the prediction coefficients $u_{f,i}$ in (13) and the derivation of the variance $2\cdot\sigma_f^2$ of the error in (12) are described in detail in section 3. m_f is the prediction order in frequency-direction.

Accordingly, at time index l, the APP estimation in time direction is characterized for subcarrier k_0 with $0 \le k_0 \le K-1$ by the metric increment

$$\gamma_l = -\frac{|Y_{k_0,l} - \hat{H}^t_{k_0,l}\cdot\hat{X}_{k_0,l}|^2}{2\cdot\sigma_t^2} + \sum_{i=0}^{2} d^i_{k_0,l}\cdot L^{\tilde{c},t,i}_{\mathrm{a},k_0,l} \quad (14)$$

with estimated channel coefficient

$$\hat{H}^t_{k_0,l} = \sum_{i=1}^{m_t} u_{t,i}\cdot\frac{Y_{k_0,l-i}}{\hat{X}_{k_0,l-i}}\ . \quad (15)$$

m_t is the prediction order in time-direction. The two one-dimensional APP estimators are concatenated as shown in Fig. 2. The output $L^{\tilde{c},f,i}_{\mathrm{d},k,l}$ of the APP estimator in frequency direction becomes the *a-priori* input $L^{\tilde{c},t,i}_{\mathrm{a},k,l}$ of the APP estimator in time direction.

2.4 Mapping

Let $\mathcal{S} = \{s_0, s_1, \ldots s_7\}$ be the symbol alphabet with $X_{k,l} \in \mathcal{S}$. Let further $\mathcal{B} = \{b_0, b_1, \ldots, b_7\}$ be the set of bit vectors that need to be mapped to the symbol alphabet, where $b_i \in \{000_2, 001_2, \ldots, 111_2\}$. $\mathcal{M} : \mathcal{B} \to \mathcal{S}$ denotes the mapping from the bit vectors to the signal points.

We use the constellation diagrams of an asymmetrical 8-QAM or an asymmetrical 8-PSK. The constellation diagram of the asymmetrical 8-QAM is depicted in Fig. 4. This constellation diagram was derived in [8] and found to give minimum BER performance among all 8-QAM constellations.

We define the following two mappings for the asymmetrical 8-QAM:

- Mapping $\mathcal{M}_{\rm QAM}0$ (from [5]):
  $\mathcal{B}_0 = \{000_2, 110_2, 010_2, 011_2, 101_2, 100_2, 001_2, 111_2\}$
- Mapping $\mathcal{M}_{\rm QAM}1$ (from [5]):
  $\mathcal{B}_1 = \{000_2, 101_2, 010_2, 111_2, 011_2, 110_2, 100_2, 001_2\}$

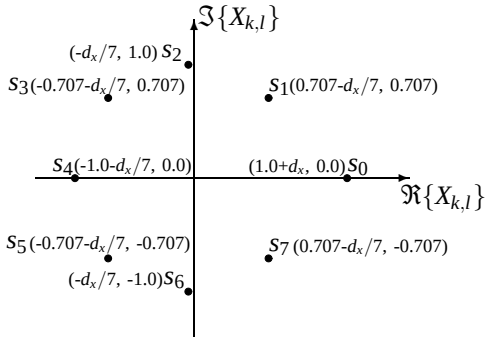

Fig. 5: Asymmetrical 8-PSK modulation scheme.

Fig. 5 shows the constellation diagram of the asymmetrical 8-PSK. We derive this constellation diagram from the symmetrical 8-PSK by moving the point s_0 from 1 to $1+d_x$. In order to achieve zero mean all the other points have to be moved in the opposite direction by $d_x/7$ as shown in Fig. 5.

We define the following two mappings for the asymmetrical 8-PSK:

- Mapping $\mathcal{M}_{\text{PSK}}0$:
  $\mathcal{B}_2 = \{000_2, 100_2, 101_2, 111_2, 110_2, 010_2, 011_2, 001_2\}$
- Mapping $\mathcal{M}_{\text{PSK}}1$:
  $\mathcal{B}_3 = \{000_2, 101_2, 011_2, 110_2, 001_2, 100_2, 010_2, 111_2\}$

3 Linear Prediction Coefficients

The approach to obtain the linear prediction coefficients in frequency (13) and time (15) is similar. Therefore, we restrict our derivation to the prediction coefficients in frequency direction.

3.1 Optimal Linear Prediction Coefficients (OLPC)

In [5], Optimal Linear Prediction Coefficients (OLPC) $u_{f,i}$ were used. For this method it is assumed, that the current state in the trellis actually was transmitted. Under this assumption, (13) can be expressed as

$$\hat{H}^f_{k,l_0} = \sum_{i=1}^{m_f} u_{f,i} \cdot \hat{H}_{k-i,l_0} \,, \tag{16}$$

whereby

$$\hat{H}_{k-i,l_0} = H_{k-i,l_0} + \frac{N_{k-i,l_0}}{\hat{X}_{k-i,l_0}} \,. \tag{17}$$

Taking (11) and (17) into account, we can compute the expected value

$$\mathrm{E}\left\{\hat{H}_{k-i,l_0} \cdot \hat{H}^*_{k-\tilde{i},l_0}\right\} = R_{f;\tilde{i}-i} + \delta_{\tilde{i}-i} \cdot \frac{N_0}{\left|\hat{X}_{k-i,l_0}\right|^2} \tag{18}$$

and the expected value

$$\mathrm{E}\left\{H_{k,l_0} \cdot \hat{H}^*_{k-i,l_0}\right\} = R_{f;i} \,. \tag{19}$$

We calculate the linear prediction coefficients solving the Wiener-Hopf equation in order to minimize the mean squared error $\mathrm{E}\left\{\left|H_{k,l_0} - \hat{H}^f_{k,l_0}\right|^2\right\}$. Therefore, the linear prediction coefficients are:

$$\left(u_{f,1}, \ldots, u_{f,m_f}\right) = \mathbf{r}_f^T \cdot \mathbf{R}_f^{-1} \tag{20}$$

Taking (19) into account, the vector $\mathbf{r}_f^T$ can be calculated as:

$$\mathbf{r}_f^T = \left(R_{f,1}, \ldots, R_{f,m_f}\right) \tag{21}$$

Using (18), we obtain the matrix $\mathbf{R}_f$ as:

$$\mathbf{R}_f = \begin{pmatrix} 1+\frac{N_0}{|\hat{X}_{k-1,l_0}|^2} & R_{f,1} & \cdots & R_{f,m_f-1} \\ R_{f,-1} & 1+\frac{N_0}{|\hat{X}_{k-2,l_0}|^2} & & R_{f,m_f-2} \\ \vdots & & \ddots & \vdots \\ R_{f,-m_f+1} & \cdots & R_{f,-1} & 1+\frac{N_0}{|\hat{X}_{k-m_f,l_0}|^2} \end{pmatrix} \tag{22}$$

The minimum mean squared error results to:

$$J_{\min,f} = 1 - \mathbf{r}_f^T \cdot \mathbf{R}_f^{-1} \cdot \mathbf{r}_f^* \tag{23}$$

Therefore, the term $2 \cdot \sigma_f^2$ in (12) yields to:

$$2 \cdot \sigma_f^2 = N_0 + J_{\min,f} \cdot \left|\hat{X}_{k,l_0}\right|^2 \tag{24}$$

As a consequence of (18), each state in the trellis has its own linear prediction coefficients and minimum mean squared error expressed in (22) and (23). Beyond, each branch in the trellis has its own variance $2 \cdot \sigma_f^2$ of the error, which directly results from (24).

3.2 Statistical Optimal Linear Prediction Coefficients (SOLPC)

In order to reduce the amount of linear prediction coefficient sets, we now derive only one coefficient set which is used for all states in the trellis. We denote these linear prediction coefficients as the Statistical Optimal Linear Prediction Coefficients (SOLPC).

To obtain these coefficients, we have to rewrite (18) as follows:

$$\mathrm{E}\left\{\hat{H}_{k-i,l_0} \cdot \hat{H}^*_{k-\tilde{i},l_0}\right\} = R_{f;\tilde{i}-i} + \delta_{\tilde{i}-i} \cdot \frac{N_0}{\beta} \,, \tag{25}$$

whereby

$$\beta^{-1} = \mathrm{E}\left\{\frac{1}{\left|\hat{X}_{k-i,l_0}\right|^2}\right\} = \mathrm{E}\left\{\frac{1}{\left|X_{k,l}\right|^2}\right\} \,. \tag{26}$$

Instead of taking $\hat{X}_{k-i,l_0}$ explicitly into account, we now use the statistical expression β. Therefore, the matrix $\mathbf{R}_f$ can now be expressed as:

$$\mathbf{R}_f = \begin{pmatrix} 1+\frac{N_0}{\beta} & R_{f,1} & \cdots & R_{f,m_f-1} \\ R_{f,-1} & 1+\frac{N_0}{\beta} & & R_{f,m_f-2} \\ \vdots & & \ddots & \vdots \\ R_{f,-m_f+1} & \cdots & R_{f,-1} & 1+\frac{N_0}{\beta} \end{pmatrix} \tag{27}$$

As a consequence of (25) and (27), all states in the trellis have the same linear prediction coefficients and

minimum mean squared error.

According to (25), we calculate the variance $2 \cdot \sigma_f^2$ of the error as follows:

$$2 \cdot \sigma_f^2 = N_0 + J_{\min,f} \cdot E_S \,, \tag{28}$$

whereby

$$E_S = \mathrm{E}\left\{ \left| \hat{X}_{k,l_0} \right|^2 \right\} = \mathrm{E}\left\{ \left| X_{k,l} \right|^2 \right\} \,. \tag{29}$$

Therefore, all branches in the trellis have the same variance $2 \cdot \sigma_f^2$ of the error.

Obviously, for symmetrical PSK constellation diagrams the optimal and the statistical optimal linear predication coefficients are identical, because $\left| X_{k,l} \right| = 1 \; \forall k,l$.

3.3 Linear Prediction Coefficients based on Averaging (ABLPC)

For our last linear prediction coefficient set we choose the pragmatic choice given in [3]. Therefore, the linear prediction coefficients are calculated as:

$$u_{f,i} = \frac{1}{m_f} \tag{30}$$

The variance $2 \cdot \sigma_f^2$ of the error is expressed as:

$$2 \cdot \sigma_f^2 = N_0 \tag{31}$$

We denote this design of the linear prediction coefficients by Averaging Based Linear Prediction Coefficients (ABLPC).

4 Simulation results

In this section, we will investigate the system performance by means of Extrinsic Information Transfer (EXIT) and BER charts. EXIT charts were introduced in [9]–[11]. They are a good tool to analyze the performance of an iterative decoding loop, such as the APP channel estimator and the convolutional decoder in our system.

Fig. 6 shows the EXIT charts for the four constellation diagrams and mappings defined in section 2.4 at $E_b/N_0 = 10\,\mathrm{dB}$. The channel parameters are $\tau_{\max} = 20\,\mu\mathrm{s}$ and $f_{D_{\max}} = 100\,\mathrm{Hz}$. For the linear prediction, $m_f = m_t = 2$ was chosen. The parameter d_x for the asymmetrical 8-PSK was set to $d_x = 0.25$.

The charts contain the characteristic curve of the convolutional decoder, and several characteristic curves of the APP channel estimator with different parameter settings. The x-axis corresponds to the mutual information input I_{A1} of the APP CE, which is mapped to a mutual information output I_{E1} by the characteristic curve of the APP CE. Likewise, the mutual information input I_{A2} of the decoder is mapped to the output I_{E2} by the characteristic curve of the decoder. Both curves allow us to conveniently investigate the improvement of the channel estimate from one iteration to the next.

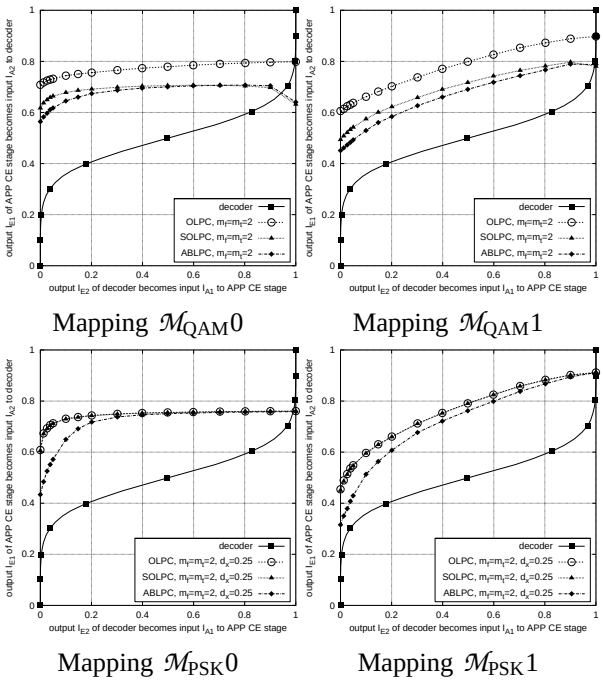

Fig. 6: EXIT chart, blind APP-CE stage and decoder for $\tau_{\max} = 20\,\mu\mathrm{s}$ and $f_{D_{\max}} = 100\,\mathrm{Hz}$ at $E_b/N_0 = 10\,\mathrm{dB}$.

The EXIT charts show that the PSK constellation is much more robust with respect to the prediction coefficient sets than the QAM scheme. Focusing on the PSK constellation, the characteristic curves for optimal linear prediction coefficients and statistical optimal linear prediction coefficients are identical and start at a higher mutual information I_{E1} than the average based linear prediction coefficient set. However, the mutual information is virtually the same for all three sets at the intersection point with the characteristic curve of the decoder. Hence, we can make up for the lower starting point by using more iterations in the iterative decoding loop. This is supported by the BER chart for Mapping $\mathcal{M}_{\mathrm{PSK}}0$ shown in Fig. 7. For an $E_b/N_0 \geq$

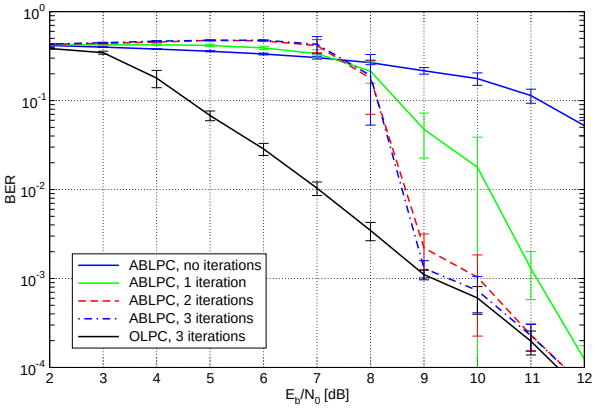

Fig. 7: BER performance of Mapping $\mathcal{M}_{\mathrm{PSK}}0$, $d_x = 0.25$, $\tau_{\max} = 20\,\mu\mathrm{s}$ and $f_{D_{\max}} = 100\,\mathrm{Hz}$.

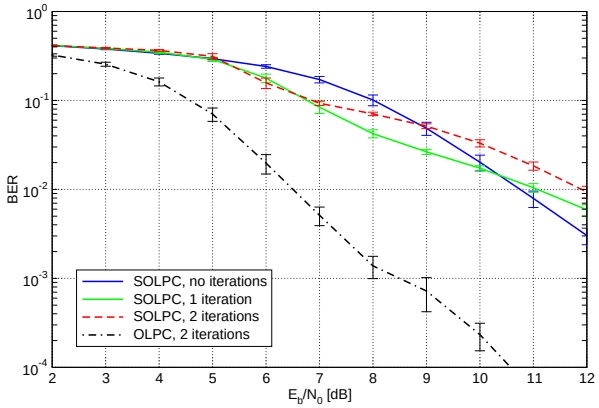

Fig. 8: BER performance of Mapping $\mathcal{M}_{\mathrm{QAM}}0$, $\tau_{\max} = 20\,\mu$s and $f_{\mathrm{D}_{\max}} = 100\,$Hz.

9 dB, the performance of the optimal linear prediction coefficients is almost matched by the coefficient set based on averaging after only two iterations.

On the other hand, the asymmetrical 8-QAM scheme is more difficult to handle as its performance depends much more on the prediction coefficients. As can be seen from the EXIT charts, the performance of OLPC is never be met by SOLPC and ABLPC. Even worse, the characteristic curves of SOLPC and ABLPC drop as the mutual information input $\mathrm{I_{A1}}$ of the APP channel estimator approaches 1. This is due to the highly variable absolute value of the signal points of the 8-QAM constellation. Consequently, with more iterations, the BER becomes worse, as can be seen in Fig. 8.

Finally, the BER performance of all mapping schemes is compared in Fig. 9 after four iterations with optimal linear prediction coefficients. Obviously, the QAM constellation outperforms the PSK constellation if optimal prediction coefficients are available. On the other hand, the discussion above revealed that the PSK constellation is much easier to handle if prediction coefficients are non-optimal. In any case, using the iterative decoding loop, the mappings $\mathcal{M}_{\mathrm{QAM}}1$ and $\mathcal{M}_{\mathrm{PSK}}1$

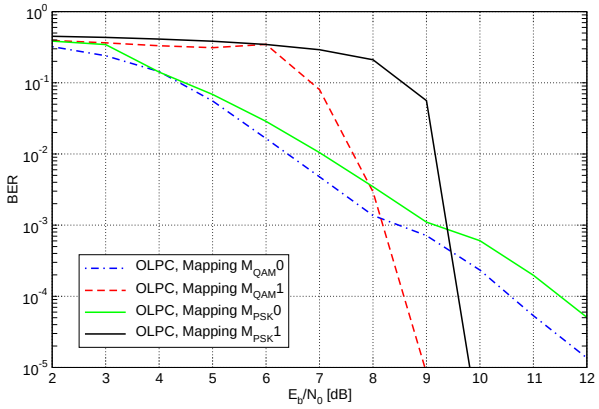

Fig. 9: BER performance of the different mappings, OLPC, 4 iterations, $d_x = 0.25$, $\tau_{\max} = 20\,\mu$s and $f_{\mathrm{D}_{\max}} = 100\,$Hz.

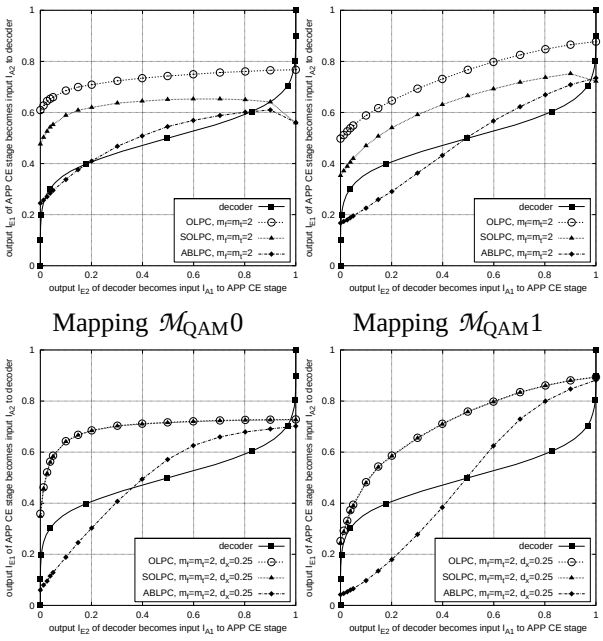

Fig. 10: EXIT chart, blind APP-CE stage and decoder for $\tau_{\max} = 40\,\mu$s and $f_{\mathrm{D}_{\max}} = 300\,$Hz at $E_\mathrm{b}/N_0 = 10\,$dB.

outperform the corresponding mappings $\mathcal{M}_{\mathrm{QAM}}0$ and $\mathcal{M}_{\mathrm{PSK}}0$ by about 2 dB at a BER of 10^{-4}.

Similar to Fig 6, Fig. 10 shows the EXIT charts for the four mappings at $E_\mathrm{b}/N_0 = 10\,$dB, but now for $\tau_{\max} = 40\,\mu$s and $f_{\mathrm{D}_{\max}} = 300\,$Hz.

Due to the high Doppler frequency and the long delay spread, the CTF varies very fast in time and frequency direction. As a consequence, the starting point at $\mathrm{I_{A1}} = 0$ of the characteristic curve for ABLPC drops to a lower value $\mathrm{I_{E1}}$. Since the characteristic curves of the APP estimation stage with ABLPC and the decoder intersect very early at a low value of $\mathrm{I_{E1}}$, there is no possibility to achieve a reasonable BER performance with any of the considered mappings. On the other hand, the EXIT charts reveal that the new channel parameters have little impact on the characteristic curves if OLPC or SOLPC is used. As a solution, an adaptive receiver could be used which needs to be capable of determining the channel's auto-correlation functions $R_{f;\Delta k}$ and $R_{t;\Delta l}$. The feasibility of such an approach was shown in [12] for pilot-based systems. Another possibility would be to use filter banks with predetermined prediction coefficient sets for selected channel scenarios.

The performance of the system can be improved by increasing the parameter d_x of the asymmetrical PSK constellation. Fig. 11 compares the characteristic curves of the APP estimator for the two values $d_x = 0.25$ and $d_x = 0.75$. Even though the starting point of the characteristic curve of the APP estimator at $\mathrm{I_{A1}} = 0$ is moved further up, it is still not possible to achieve a reasonable BER performance at $E_\mathrm{b}/N_0 = 10\,$dB. Again,

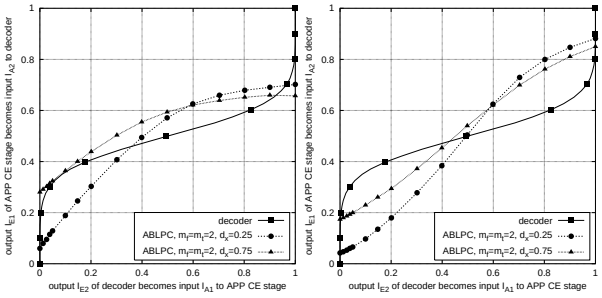

Mapping $\mathcal{M}_{\mathrm{PSK}}0$ Mapping $\mathcal{M}_{\mathrm{PSK}}1$

Fig. 11: EXIT chart, blind APP-CE stage and decoder for $\tau_{\max} = 40\,\mu\mathrm{s}$ and $f_{\mathrm{D}_{\max}} = 300\,\mathrm{Hz}$ at $E_\mathrm{b}/N_0 = 10\,\mathrm{dB}$.

the reason is that the intersection with the characteristic curve of the decoder occurs at a very low mutual information I_{E1}.

As a last possibility to improve performance with ABLPC, we modify the prediction orders m_f and m_t. So far, m_f and m_t were set to 2, corresponding to a mean value calculation. As a second possibility, we will investigate $m_f = m_t = 1$, which assumes that the CTF is approximately constant for adjacent subcarriers and consecutive OFDM-symbols (the same assumption was already made in [4]).

Fig. 12 depicts the EXIT charts for the two PSK mappings, $m_f = m_t = 1$ and $m_f = m_t = 2$. The diagrams show that the performance of the system improves by choosing $m_f = m_t = 1$, even though the noise has a bigger impact for smaller prediction orders. Obviously, the assumption of an approximately constant CTF for adjacent subcarriers and consecutive OFDM-symbols is more appropriate than a mean value calculation. This is a very nice result, since the complexity of the APP decoder reduces by a factor of 8 in the case of an 8-ary modulation scheme if the prediction order is reduced by 1.

The BER chart in Fig. 13 for mapping $\mathcal{M}_{\mathrm{PSK}}0$ confirms the observations from the EXIT charts. With $m_f = m_t = 1$ we can achieve a BER on the order of 10^{-3} at $E_\mathrm{b}/N_0 = 10\,\mathrm{dB}$, whereas a much higher E_b/N_0

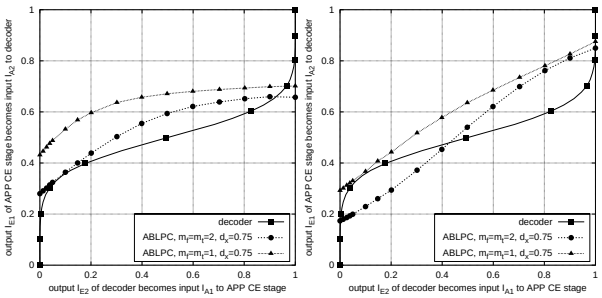

Mapping $\mathcal{M}_{\mathrm{PSK}}0$ Mapping $\mathcal{M}_{\mathrm{PSK}}1$

Fig. 12: EXIT chart, blind APP-CE stage and decoder for $\tau_{\max} = 40\,\mu\mathrm{s}$ and $f_{\mathrm{D}_{\max}} = 300\,\mathrm{Hz}$ at $E_\mathrm{b}/N_0 = 10\,\mathrm{dB}$.

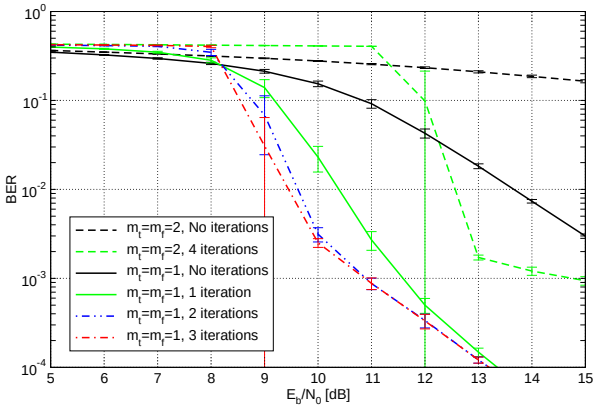

Fig. 13: BER performance of Mapping $\mathcal{M}_{\mathrm{PSK}}0$, $d_x = 0.75$, ABLPC, $\tau_{\max} = 40\,\mu\mathrm{s}$ and $f_{\mathrm{D}_{\max}} = 300\,\mathrm{Hz}$

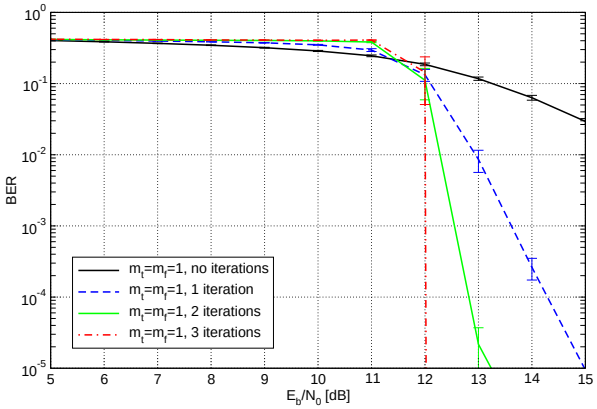

Fig. 14: BER performance of Mapping $\mathcal{M}_{\mathrm{PSK}}1$, $d_x = 0.75$, ABLPC, $\tau_{\max} = 40\,\mu\mathrm{s}$ and $f_{\mathrm{D}_{\max}} = 300\,\mathrm{Hz}$.

is required if $m_f = m_t = 2$.

As expected from the EXIT charts, a higher E_b/N_0 is needed for the same BER with mapping $\mathcal{M}_{\mathrm{PSK}}1$. This is shown in Fig. 14. However, since the characteristic curves of the APP estimator and the decoder intersect at a higher mutual information I_{E1} for mapping $\mathcal{M}_{\mathrm{PSK}}1$, the achievable BER for higher E_b/N_0 is better than that of mapping $\mathcal{M}_{\mathrm{PSK}}0$. This fact manifests itself in the turbo-cliff at $E_\mathrm{b}/N_0 = 12\,\mathrm{dB}$, where the BER rapidly drops below the BER with mapping $\mathcal{M}_{\mathrm{PSK}}0$.

5 Conclusion

We studied the impact of prediction coefficients of a totally blind APP channel estimator in a mobile environment. Our results prove that excellent BER performance is achievable if the receiver has knowledge of the channel's auto-correlation functions, both with asymmetrical 8-QAM and asymmetrical 8-PSK. In the case of asymmetrical 8-PSK, the same performance can be achieved even in case this knowledge is not available. This is realized with a simple non-adaptive

first-order predictor at the receiver side. Other modulation schemes, such as asymmetrical 8-QAM schemes, require adaptive receiver designs, which are capable of tracking the auto-correlation functions of the channel.

References

[1] P. Höher, S. Kaiser, and P. Robertson, "Two–dimensional pilot–symbol–aided channel estimation by Wiener filtering," in *ICASSP*, Munich, Germany, April, 1997, pp. 1845–1848.

[2] "Digital video broadcasting (DVB); framing structure, channel coding and modulation for digital terrestrial television (DVB-T)," *European Telecommunication Standard, ETS 300744*, March 1997.

[3] F. Sanzi and S. ten Brink, "Iterative channel estimation and decoding with product codes in multicarrier systems," in *Proc. IEEE Vehicular Tech. Conf. (VTC–Fall)*, Boston, USA, September, 2000, pp. 1338–1344.

[4] M. Necker and G. Stüber, "Totally blind channel estimation for OFDM over fast varying mobile channels," in *Proc. IEEE Intern. Conf. on Comm.*, New York, USA, April, 2002, pp. 421–425.

[5] F. Sanzi and M. C. Necker, "Totally blind APP channel estimation with higher order modulation schemes," in *Proc. IEEE Vehicular Tech. Conf. (VTC–Fall)*, Orlando, USA, October, 2003.

[6] P. Höher, "A statistical discrete-time model for the WSSUS multipath channel," *IEEE Trans. on Veh. Tech.*, vol. 41, no. 4, pp. 461–468, November, 1992.

[7] F. Sanzi, S. Jelting, and J. Speidel, "A comparative study of iterative channel estimators for mobile OFDM systems," *IEEE Trans. on Wireless Comm.*, vol. 2, no. 5, September, 2003.

[8] G. J. Foschini, R. D. Gitlin, and S. B. Weinstein, "Optimization of two-dimensional signal constellations in the presence of gaussian noise," *IEEE Trans. on Comm.*, vol. 22, no. 1, pp. 28–38, January, 1974.

[9] S. ten Brink, "Iterative decoding trajectories of parallel concatenated codes," in *Proc. 3rd IEEE/ITG Conf. on Source and Channel Coding*, Munich, Germany, January, 2000, pp. 75–80.

[10] ——, "Design of serially concatenated codes based on iterative decoding convergence," in *Proc. 2nd International Symposium on Turbo Codes*, Brest, France, September, 2000, pp. 319–322.

[11] ——, "Convergence behavior of iteratively decoded parallel concatenated codes," *IEEE Trans. on Comm.*, vol. 49, no. 10, pp. 1727–1737, October, 2001.

[12] M. Necker, F. Sanzi, and J. Speidel, "An adaptive wiener-filter for improved channel estimation in mobile OFDM-systems," in *Proc. IEEE Intern. Symp. on Signal Proc. and Inf. Tech. (ISSPIT)*, Cairo, Egypt, December, 2001, pp. 213–216.